Spin relaxation in inhomogeneous quantum dot arrays studied by electron spin resonance

A. F. Zinovieva,* N. P. Stepina, A. I. Nikiforov, A. V. Nenashev, and A. V. Dvurechenskii
Institute of Semiconductor Physics, SB RAS, 630090 Novosibirsk, Russia

L. V. Kulik
Institute of Chemical Kinetics and Combustion, SB RAS, 630090 Novosibirsk, Russia

M. C. Carmo and N. A. Sobolev
Departamento de Fisica and I3N, Universidade de Aveiro, 3810-193 Aveiro, Portugal
(Received 11 October 2013; revised manuscript received 1 January 2014; published 16 January 2014)

Electron states in an inhomogeneous Ge/Si quantum dot array with groups of closely spaced quantum dots were studied by the conventional continuous-wave electron spin resonance and spin-echo techniques. We have found that the existence of quantum dot groups allows increasing the spin relaxation time in the system. The created structures permit us to change the effective localization radius of electrons by an external magnetic field. With the localization radius being close to the size of a quantum dot group, we obtain a fourfold increase in the spin relaxation time T_1 as compared to conventional homogeneous quantum dot arrays. This effect is attributed to an averaging of the local magnetic fields produced by ^{29}Si nuclear spins and a stabilization of the S_z polarization during the electron back-and-forth motion within a quantum dot group.

DOI: 10.1103/PhysRevB.89.045305 PACS number(s): 73.21.La, 03.67.Lx, 72.25.Rb

I. INTRODUCTION

Electron spins in quantum dots (QDs) can be considered as promising candidates for the implementation of quantum computation ideas and spintronics devices [1,2]. The main parameter indicating the applicability of a system to quantum computation is the spin coherence time. An extremely long spin lifetime is observed in zero-dimensional structures due to a strong confinement in all three dimensions [3]. An especially great potential for a long coherence time is expected in the Ge/Si system with quantum dots. The electrons in this system are localized in strained Si regions, where the spin-orbit (SO) coupling is very weak. However, recent investigations of spin decoherence by the spin echo method in the Ge/Si QD system [4] demonstrated that the spin relaxation times are unexpectedly short ($\sim$10 μs). It was suggested that the reason of such an intensive spin relaxation consists of the appearance of effective magnetic fields during electron tunneling between quantum dots. These magnetic fields (Rashba fields) [5] originate from the spin-orbit interaction and arise due to the absence of mirror symmetry of the localizing potential for an electron in the vicinity of a Ge QD. Spin relaxation occurs through a stochastic spin precession in effective magnetic fields during random tunneling between QDs (an analog of the Dyakonov-Perel mechanism for delocalized carriers [6]). Obviously, the suppression of the tunneling in an array of well separated quantum dots allows us to eliminate the existence of in-plane fluctuating magnetic fields. In this case the hyperfine interaction with ^{29}Si nuclear spins comes into force and determines the spin relaxation time. If the tunneling is suppressed not by the spatial separation of QDs, but by the Coulomb repulsion [7], the anisotropic exchange interaction can also control the spin relaxation process.

The efficiency of each mechanism depends in different ways on the localization degree of electrons. By changing the tunnel coupling between quantum dots (by changing their density) and, correspondingly, the localization degree of electrons, it is possible to alter the relative contribution of different mechanisms. With increasing electron localization radius the contribution of hyperfine interaction becomes smaller due to an averaging-out of different orientations of nuclear spins. A related increase of the relaxation time occurs until the moment when the wave function overlapping provides the hopping between neighboring localization centers. In these conditions, the Dyakonov-Perel mechanism begins to control the spin relaxation process [8]. The longest spin relaxation time is expected right before the point where the Dyakonov-Perel mechanism comes into force. A similar effect was detected in n-type GaAs, where a threefold increase of the spin relaxation time was obtained in the vicinity of the metal-to-insulator transition [9].

In self-assembled tunnel-coupled QD structures it is hard to get a gradual change of the localization radius by changing the QD array density. Stochastic nucleation of QDs upon the Stranski-Krastanow growth mode [10] leads to the formation of regions with a high local density of QDs. In such regions, a strong tunnel coupling between the dots results in an intense spin relaxation through the Dyakonov-Perel mechanism. However, under certain conditions, the existence of groups of closely located QDs can provide not a decrease, but rather an increase of the spin relaxation time. First, the QD groups should be well separated from each other. In this case, the effective magnetic fields can be averaged due to the electron back-and-forth motion within each QD group. Secondly, the QDs inside a group should have a strong tunnel coupling providing the effective localization radius comparable to the QD group size. As a result, the averaging of local magnetic fields related to nuclear spins will take place.

The present work is devoted to an electron spin resonance (ESR) study of inhomogeneous QD arrays, where the

*aigul@isp.nsc.ru

averaging of the Rashba and hyperfine fields inside QD groups is expected to provide a long spin relaxation time. We succeeded in creating an experimental structure containing well separated groups of QDs with a large electron localization radius. The coupling between QDs and, consequently, the electron localization radius in the structures under study turned out to be dependent on the external magnetic field orientation. A fourfold increase of the spin relaxation time as compared to the previous data for dense homogeneous QD arrays [4] has been detected at a special orientation of the magnetic field, where the electron localization radius was close to the QD group size.

II. SAMPLES AND EXPERIMENTAL CONDITIONS

The samples were grown by molecular-beam epitaxy on n-Si(001) substrates with a resistivity of 1000 Ω cm. To increase the response from the sample, we have grown 6 layers of Ge nanoclusters separated by 30 nm Si layers. Each QD layer was formed by the deposition of 7 monolayers of Ge at the temperature $T = 550\,^{\circ}$C. On top of the structure, a 0.3 μm epitaxial n-Si layer (Sb concentration $\geqslant 10^{17}$ cm^{-3}) was grown; an equal layer was deposited also below the QD layers. Scanning tunneling microscopy (STM) of the structure with a single QD layer uncovered by Si shows a bimodal distribution of QDs (hut and dome clusters) (Fig. 1). The density of dome clusters is $\sim 10^{10}$ cm^{-2}, their typical base width is $l = 50$ nm, and the height is $h = 10$ nm. The hut clusters are distributed between the dome clusters with a density of $\sim 10^{11}$ cm^{-2}, their typical base width is $l = 15$ nm, and the height is $h = 1.5$ nm.

The obtained size of dome clusters has to provide a strong localization of electrons at the apexes of domes with a small localization radius. To increase the latter, we used a temperature of 500 °C for the overgrowth of the QDs allowing us to transform the dome clusters into disk-like ones without a strong Ge-Si intermixing inside the QDs. Cross-section transmission electron microscopy (TEM) images show that the height of the disk-like dots does not exceed 3 nm in the experimental structure. These dots, as well as the original domes, are characterized by the absence of mirror symmetry

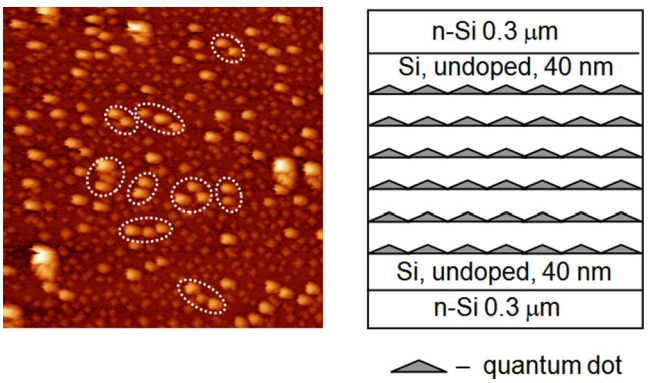

FIG. 1. (Color online) Left panel: STM of the uncovered sample with two shapes of QDs (hut clusters and dome clusters), 1 μm × 1 μm image. Right panel: A schematic structure of the investigated sample. The examples of quantum dot groups are indicated by dashed line loops.

due to a difference between the smeared top and the sharper bottom of the QDs. After such an overgrowth the localization radius is expected to be comparable to the lateral QD size.

STM data show a nonhomogenous in-plane distribution of *dome* clusters and the existence of groups of 2–3 closely spaced nanoclusters, on average (Fig. 1). A sufficient tunneling coupling between them allows the electron wave function to spread over the whole QD group and promotes a further increase of the electron localization radius.

Hut clusters in these structures cannot be centers of localization because the electron binding energy on huts is very small (∼10 meV) [11]. Recently, to provide the localization of electrons on hut clusters, stacked structures with four layers of Ge QDs were grown [12]. The distances between the QD layers were 3 nm and 5 nm, and this resulted in an effective deepening of the potential well near the hut clusters due to the accumulation of strain from different QD layers. In the structure under study, the distance between the QD layers is 30 nm, so that the strain accumulation does not occur.

The ESR measurements were performed with a Bruker Elexsys 580 X-band EPR spectrometer using a dielectric Bruker ER-4118 X-MD-5 cavity. The samples were glued on a quartz holder, and the entire cavity and the sample were maintained at a low temperature in a helium flow cryostat (Oxford CF935). The interfering ESR signal from dangling bonds ($g = 2.0055$) was eliminated using the passivation of structures with atomic hydrogen before measurements. To increase the number of detectable spins, a sandwiched specimen was prepared. The samples were thinned by acid etching down to 150–250 μm. After thinning, the samples were glued together; finally, the specimen composed of 4–5 wafers was investigated.

The spin echo measurements were carried out at a temperature of 4.5 K in a resonance magnetic field $H = 3470$ Oe (which could be slightly varied by ±5 Oe depending on the resonance conditions) with the orientation corresponding to the narrowest ESR line width, $\theta = 30^{\circ}$, where θ is the angle between the magnetic field and the growth direction of the structure, [001]. A two-pulse Hahn echo experiment ($\pi/2$–τ–π–τ echo) was used to measure T_2 (a detailed explanation can be found in Ref. [13]). In order to observe the longitudinal spin relaxation (corresponding to the T_1 time), a different pulse sequence is applied (π–τ–$\pi/2$–T–π–T echo). The first π pulse rotates the magnetization opposite to its thermal equilibrium orientation, where the interaction with the environment causes the spins to relax back to the initial orientation parallel to **H**. After the time τ, a $\pi/2$ pulse followed by another π pulse is used to observe the Hahn echo. In the first and second type of experiment, the durations of the $\pi/2$ and π pulses were 60 ns and 120 ns, respectively; the interpulse time in the second experiment was kept at $T = 200$ ns.

III. RESULTS

The ESR spectra measured at different directions of the magnetic field are shown in Fig. 2, where $\theta = 0^{\circ}$ corresponds to the magnetic field applied parallel to the growth direction Z. At $\theta = 0^{\circ}$ the ESR line has the most symmetrical shape, and its profile is close to a Gaussian. The line asymmetry becomes more pronounced with increasing angle θ, and the line shape

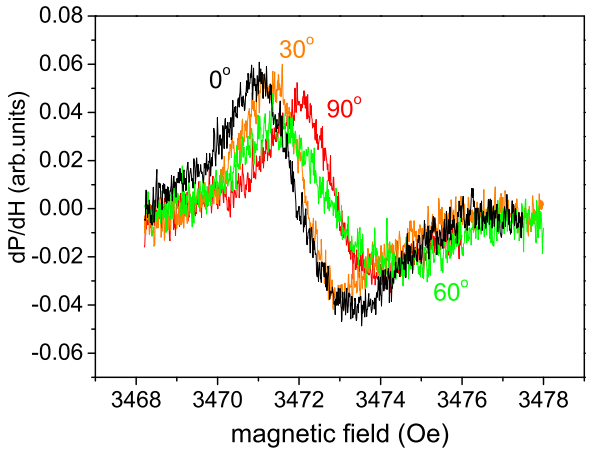

FIG. 2. (Color online) ESR spectra at different orientations of magnetic field. For $\theta = 0^\circ$ the magnetic field is parallel to the growth direction of the structure [001]; $\theta = 90^\circ$ corresponds to magnetic field applied along the crystallographic direction [110].

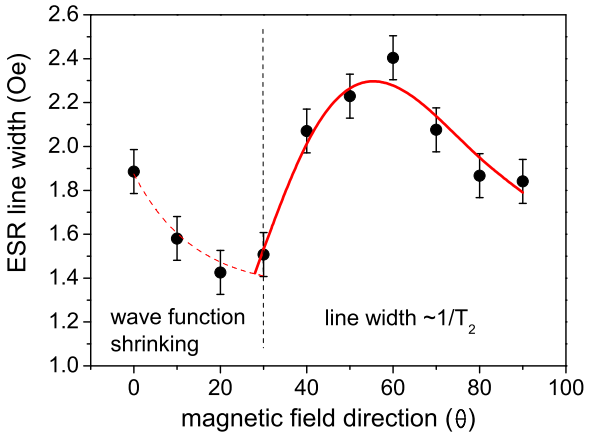

FIG. 4. (Color online) Experimental angular dependence of the ESR line width and the corresponding theoretical approximation [Eq. (6)] (solid line) for the structure under study. For $\theta = 0^\circ$ the magnetic field is parallel to the growth direction of the structure.

tends to a Lorentzian already at $\theta = 10^\circ$. The line shape analysis performed at $\theta = 30^\circ$ is shown in Fig. 3. A careful examination shows that the ESR line represents a sum of an absorption line (dotted) and a dispersion line (dashed). The rotation of the sample in the magnetic field results in a change of the width and position of the resonance line. The orientation dependence of the ESR line width for the structure under study is demonstrated in Fig. 4. When the external magnetic field deviates from the growth direction up to $\theta \approx 30^\circ$, the ESR line width sharply decreases from $\Delta H = 1.9$ Oe to $\Delta H = 1.4$ Oe. A further tilt of the magnetic field leads to a line broadening up to a maximum of $\Delta H = 2.4$ Oe at $\theta = 60^\circ$. For the in-plane magnetic field, the ESR line width is narrowed again down to $\Delta H = 1.8$ Oe. Such a nonmonotonous behavior is unusual for electrons in a two-dimensional system and has not been observed to date.

The angular dependence of the g factor is shown in Fig. 5. At small angles (up to $\theta = 30^\circ$) the g factor slightly varies near $g = 1.9994(5)$. Between $\theta = 30^\circ$ and $\theta = 40^\circ$ the g factor value jumps to $g = 1.9992$ and remains nearly constant up to $\theta = 90^\circ$.

The data of spin echo measurements performed at $\theta = 30^\circ$, when the smallest ESR line width is observed, are shown in Figs. 6 and 7. According to the results of a two-pulse Hahn echo experiment, the spin echo behavior can be described by a superposition of two exponentially decaying functions:

$$M(t) = M_{x,y}^{(1)} \exp\left(-2\tau/T_2^{(1)}\right) + M_{x,y}^{(2)} \exp\left(-2\tau/T_2^{(2)}\right), \tag{1}$$

where $M(0) = M_{x,y}^{(1)} + M_{x,y}^{(2)}$ is the lateral (in QD plane) magnetization after a $\pi/2$ pulse. The decay parameters yield two times the spin dephasing: $T_2^{(1)} \approx 0.26$ μs and $T_2^{(2)} \approx 1.5$ μs.

The analysis of the inversion signal recovery measured in three-pulse echo experiments shows a nonexponential behavior (Fig. 7). The experimental curve can be described by the superposition of two functions:

$$M(t) = M_{0z} - M_z^{(1)} \exp\left(-\tau/T_1^{(1)}\right) - M_z^{(2)} \exp\left(-\tau/T_1^{(2)}\right), \tag{2}$$

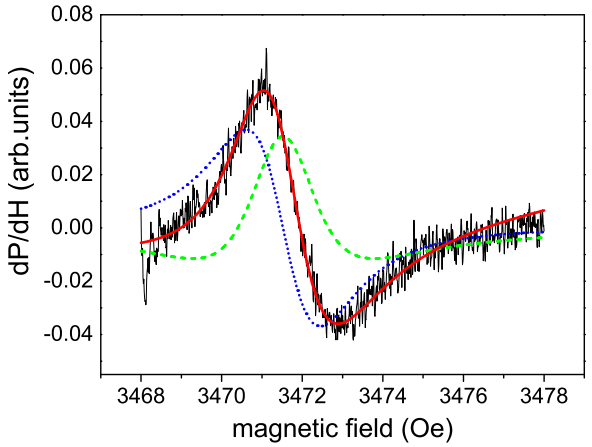

FIG. 3. (Color online) Analysis of the ESR line shape for $\theta = 30^\circ$. The solid line represents the sum of an absorption line (dotted), and a dispersion line (dashed).

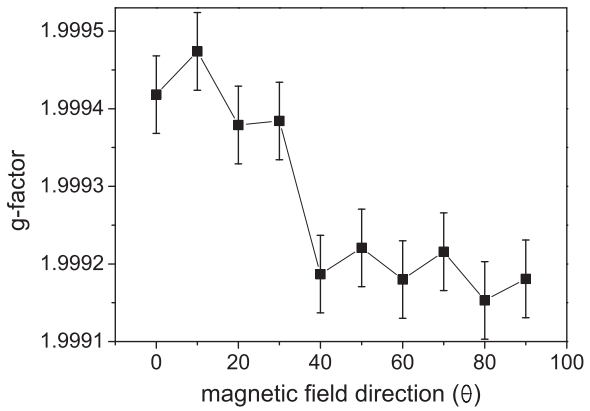

FIG. 5. Angular dependence of the electron g factor for the structure under study. For $\theta = 0^\circ$ the magnetic field is parallel to the growth direction of the structure.

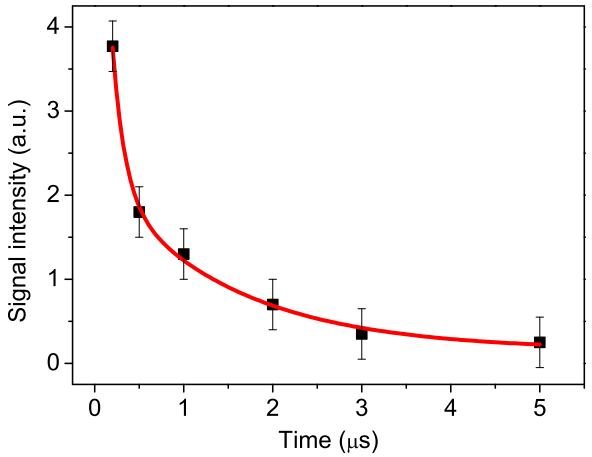

FIG. 6. (Color online) Results of two-pulse spin echo experiments performed at $\theta = 30^\circ$ (points) and the respective approximation by the superposition of two exponential functions, Eq. (1) (solid line). The corresponding microwave pulse sequence is $\pi/2$–τ–π–τ echo.

where M_{0z} is the equilibrium magnetization, $M_{0z} = M_{0z}^{(1)} + M_{0z}^{(2)}$, $M_z^{(1,2)} = M_{0z}^{(1,2)} - M_z^{(1,2)}(0)$, and $M_z(0) = M_z^1(0) + M_z^2(0)$ is the magnetization just after applying an inverting π pulse. In accordance with this equation, at the beginning the magnetization recovers very fast. After some time, a fraction of spins returns to the equilibrium state, and the recovery rate becomes much slower. The characteristic times obtained by fitting the experimental data are $T_1^{(1)} \approx 2\ \mu$s and $T_1^{(2)} \approx 35\ \mu$s. All values of the spin relaxation times were determined with an uncertainty of $\pm 20\%$.

IV. DISCUSSION

To explain the experimental results obtained in the present work, we propose the following model (see Fig. 8). The electrons are suggested to be localized mainly in the groups of closely spaced QDs containing 2–3 dots on average (see STM data). During the overgrowth the QDs lose their apexes and transform into the disk-like shape QDs. As a result, the electron localization radius can become comparable with the QD lateral size. Additional barriers for electrons limiting the electron motion in the XY directions in the Si layer arise due to the existence of regions with a nonzero Ge content. These regions are located over the edges along the perimeter of the QDs, and they are formed according to the formation mechanism of SiGe rings described in Ref. [14]. Thus, the electron localization radius can be taken to be about 50 nm for a spatially isolated single QD. In the case of a group of closely spaced QDs, the separating SiGe barriers between the dots inside the group are absent because of energetically unfavorable positions of Ge atoms between QDs due to a high strain [15]. SiGe barriers remain only along the external borders of QD groups. Then the electron wave function can spread to the size of the QD group, $l \sim 100$–150 nm. Since the confinement of the electrons is not too strong, the tails of electron wave functions from different QD groups can overlap, providing hopping between the QD groups. The external magnetic field applied along the growth direction can considerably change the described picture. The magnetic length $\lambda = \sqrt{c\hbar/eH}$ is in our experimental setup ($H = 3470$ Oe) about 45 nm, which is comparable with the electron localization radius for a single QD. In these conditions, the magnetic field leads to depression of the electron wave function tails [16], resulting in an enhancement of electron localization. Thus, the perpendicular magnetic field suppresses the transitions between QD groups and decreases the electron localization radius in the QD group down to the size of an individual QD. Nevertheless, the transitions between QDs inside the groups still persist due to a small distance between the QDs. With the deviation of the magnetic field from the growth direction the wave function shrinking effect vanishes and the probability of electron transitions

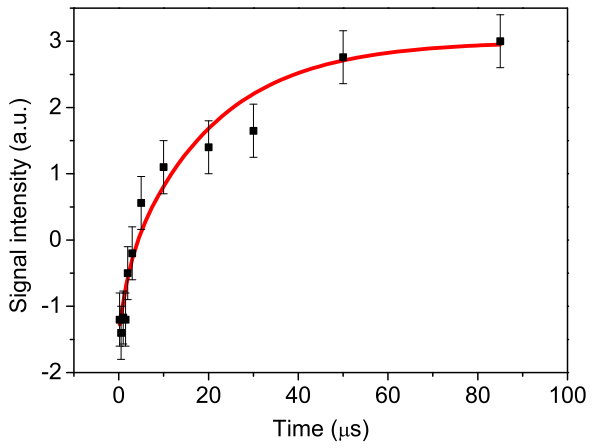

FIG. 7. (Color online) Amplitude of the inversion-recovery signal versus interpulse delay τ [symbols are experimental data, the solid line is the approximation by Eq. (2)]. The corresponding microwave pulse sequence is π–τ–$\pi/2$–T–π–T echo. The experiments are performed at $\theta = 30^\circ$.

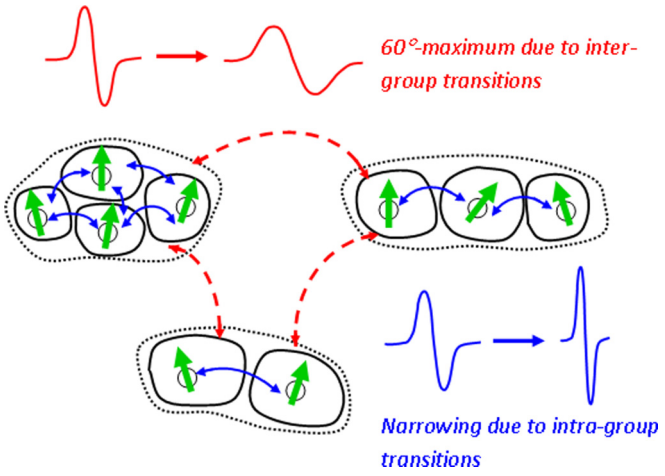

FIG. 8. (Color online) Illustration of the hopping model for the structure under study. Hopping transitions inside the QD groups provide a narrowing of the ESR line with the deviation of magnetic field from $\theta = 0^\circ$ to $\theta = 30^\circ$. Hopping transitions between the QD groups provoke spin relaxation through the spin precession mechanism and yield a special orientation dependence of the ESR line width in the range of $\theta \in \{30^\circ$–$90^\circ\}$.

between dots increases. The conductivity in local areas (QD groups) becomes higher. In the experiment, this corresponds to the appearance of a noticeable dispersion signal and to an enhancement of the asymmetry of the ESR line (the ESR line acquires a nearly Dysonian shape [17]). A similar effect was observed for SiGe/Si/SiGe structures with a two-dimensional (2D) electron gas [18].

At the same time, the increase of the effective electron localization radius causes an averaging of the local magnetic fields induced by nuclear spins and a smoothing of the QD parameter differences within a QD group. As a result, the narrowing of the ESR line upon deviation of the magnetic field from $\theta = 0^\circ$ to $\theta = 30^\circ$ is observed. The minimum of the ESR line width at $\theta = 30^\circ$ indicates that the electron localization radius reaches the size of the QD group, and a full averaging inside each group takes place. A further increase of the electron localization radius leads to an enhancement of the hopping between the groups and a decrease of the spin lifetime through the Dyakonov-Perel spin relaxation mechanism.

The decreasing spin relaxation time affects the ESR line width. From $\theta = 30^\circ$ on the broadening due to the spin relaxation, $\Delta H \cong 1/T_2$, exceeds the nonhomogeneous broadening, and the further orientation dependence of the ESR line width is controlled by the spin relaxation time.

It should be noted that there is another mechanism which can provide the anisotropy of the ESR line width, viz., relaxation assisted by the spin-phonon interaction. This mechanism can be effective due to the lack of phonon bottleneck in our structures with large QD sizes resulting in small confinement energies of electrons. In this case the anisotropy of spin relaxation processes is determined by the shape asymmetry of disk-like QDs. Their lateral size is one order of magnitude larger than their height, therefore only k_x- and k_y-phonon waves effectively influence the spin. However, the experimentally observed maximum of the ESR line width at $\theta = 60^\circ$ cannot be described in the framework of the spin-phonon interaction model [19], which should yield a monotonous orientation dependence of the ESR line width.

The Dyakonov-Perel mechanism allows describing the nonmonotonous behavior of the ESR line width on the assumption that τ_h depends on the magnetic field. This dependence, determined in the framework of the hopping model [19], can be described as an exponential,

$$\tau_h = \tau_0 \exp\left(\alpha H_z^m\right), \tag{3}$$

where H_z is the projection of the magnetic field to the growth direction; the coefficient m can be equal to $m = 1/2$ or $m = 2$ for the case of strong or weak magnetic fields, respectively. For intermediate fields, $\lambda \sim l$, this coefficient can take a value in the range $\frac{1}{2} < m < 2$ (Ref. [16]).

The spin relaxation time T_2 in the framework of the Redfield theory [20] is given by the following expression:

$$\frac{1}{T_2} = \gamma^2 \delta H_y^2 \sin^2\theta \tau_h + \frac{1}{2T_1}, \tag{4}$$

with

$$\frac{1}{T_1} = \gamma^2\left(\delta H_x^2 + \delta H_y^2 \cos^2\theta\right)\frac{\tau_h}{1+\omega_0^2\tau_h^2}, \tag{5}$$

where the correlation time of spin-orbit field fluctuations τ_c was replaced by the hopping time τ_h; ω_0 is the Larmor frequency; δH_x, δH_y are the components of the effective magnetic field δH.

Thus, using Eq. (3) for τ_h, we obtain the following expression describing the orientation dependence of the ESR line width:

$$\Delta H = B \exp(A \cos^m\theta)\left(\sin^2\theta + \frac{1+\cos^2\theta}{1 + C\exp(2A\cos^m\theta)}\right), \tag{6}$$

where $B = \gamma \delta H_y^2 \tau_0$, $A = \alpha H^m$, $C = \omega_0^2\tau_0^2$. The experimental data $\Delta H(\theta)$ in the range of $\theta \in [30^\circ, 90^\circ]$ are well approximated by this expression (Fig. 4) with $m = 3/2$, $A = 1.52$, $B = 1.78$, $C = 795.2$. The obtained coefficient m corresponds to the case of intermediate magnetic fields ($\lambda \sim l$) that argues for the accepted hopping model with τ_h depending on the magnetic field.

The magnitude of the effective magnetic field δH, estimated from the B coefficient, turns out to be $\approx$15 Oe. This value is twice as small as that determined in our previous work [21] for hut clusters with the aspect ratio $h/l = 0.1$. It is known [22] that in a QD system the effective magnetic field depends on the h/l value: the higher the aspect ratio, the larger the δH value. For the QDs under study the aspect ratio is about 0.05, therefore the effective magnetic field proved to be smaller.

The spin echo data are in a good agreement with the proposed model implying the existence of closed groups of quantum dots being the centers of electron localization. The experimental spin polarization behavior shows that the spin relaxation occurs in two stages: a rapid and a slow one. To understand the origin of this two-stage spin dynamics, we simulated the spin relaxation process in a ring-shaped group of QDs. The model includes a strong tunnel coupling between quantum dots in the circle. Hopping between any neighboring QDs is permitted with equal probability for the back-and-forth motion. Each tunneling transition is accompanied by a spin rotation by a small fixed angle $\alpha = 0.1$. The direction of the rotation axis is defined by the product $[\mathbf{n} \times \mathbf{e_z}]$, where $\mathbf{n}$ is the tunneling direction, and $\mathbf{e_z}$ is the QD growth direction. The external magnetic field is applied along $\mathbf{e_z}$ and provides the Larmor precession between tunneling events. The time intervals between tunneling events are distributed exponentially with a mean value τ_h. The spin relaxation caused by the interaction with phonons and nuclear spins was not taken into consideration. The transport was simulated by the Monte Carlo method for different numbers of QDs in the circle. The simulation results for a ring consisting of 10 quantum dots are demonstrated in Fig. 9. The two-stage spin dynamics is clearly seen. It turned out that this effect depends on the relation between the hopping time τ_h and the Larmor frequency ω_l. The two-stage dynamics is observed when $\omega_l\tau_h \ll 1$. For example, the data in Fig. 9 were obtained at $\omega_l\tau_h = 0.1$. The first stage of spin relaxation is related to the processes of electron spreading over the group of QDs. At this stage the loss of spin polarization occurs due to the precession in the effective magnetic field during the tunneling between dots. The spin dynamics at the second stage is defined by the phase breaking of the Larmor precession during a random walk along

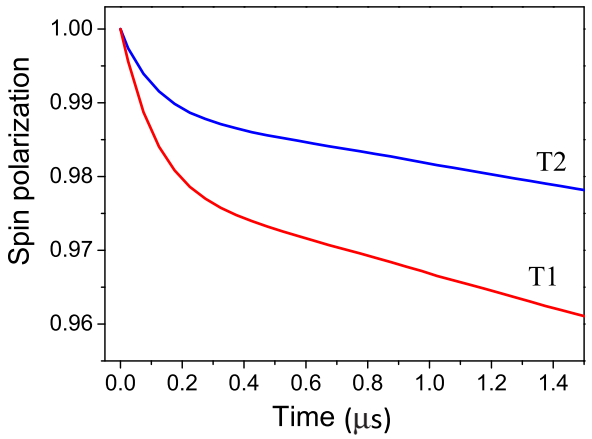

FIG. 9. (Color online) Results of a spin relaxation simulation in a closed ring-shaped group of QDs. The number of QDs in the ring is $n = 10$. The hopping time is taken as $\tau_h = 10^{-11}$ s; the Larmor frequency is one order of magnitude smaller, $\omega = 10^{10}$ s^{-1}. A two-stage dynamics is observed.

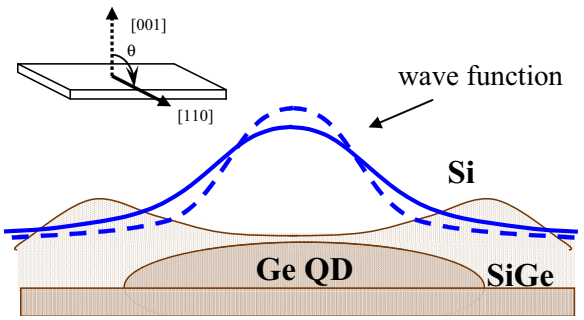

FIG. 10. (Color online) Schematic picture of the electron wave function penetration into the SiGe barrier surrounding a Ge quantum dot at different magnetic field orientations. The dashed line represents the wave function at $\theta = 0°$, the solid line corresponds to the wave function at $\theta = 90°$. The SiGe barrier is formed due to Ge diffusion to the QD periphery during the growth of the Si cover layer [14]. The case of a single quantum dot is depicted for simplicity.

the QD ring. Generally speaking, this stage of spin relaxation can be ruled by the spin-phonon or hyperfine interaction as well, if one includes them in the consideration. The absence of two-stage dynamics in the case of $\omega_l \tau_h \geqslant 1$ can be understood by the simple consideration of the spin behavior in a reference frame rotating with the Larmor frequency. The randomness of hopping between dots leads to an averaging of the effective magnetic field ($\langle \delta H \rangle = 0$) and elimination of spin relaxation at the first stage of the electron extension over the QD group. According to the simulation results, the first rapid stage is characterized by a special relation between the longitudinal and transverse spin relaxation times T_1 and T_2, akin to a 2D system with the absence of mirror symmetry, viz., $T_2 \approx 2T_1$. Such a relation was obtained by spin echo measurements for 2D electron gas structures [23] and for dense homogeneous QD arrays [4], and follows from the in-plane arrangement of the fluctuating magnetic fields δH. Also we have verified the presence of two-stage spin dynamics in QD clusters with other spatial arrangements; for example, QD lines containing a few dots. The described general features are well preserved upon changing only the numerical values of T_1 and T_2.

In T_2 measurements the first stage is characterized by $T_2 \approx 0.26\ \mu$s. Based on the simulation results one can expect the same shortness for T_1. However, the three-pulse method has limitations in the measurements of such short times. The difference between the durations of the pulse sequences in the T_1 and T_2 experiments is comparable to the duration of the first rapid stage of spin relaxation, which makes difficult the study of the beginning of the S_z relaxation.

The second stage of spin relaxation has the characteristic times $T_1 = 2\,\mu$s and $T_2 = 1.5\,\mu$s. Here, the special relation $T_2 \approx 2T_1$ is not fulfilled because of the presence of some additional spin relaxation mechanisms, for example, Larmor precession phase breaking during a random walk along the QD group, or another one. The presence of long-living spin polarization with the relaxation time $T_1 \approx 35\ \mu$s is attributed to some stabilization of the S_z component taking place during the electron movement within a closed QD group. According to the simulation results at a high hopping frequency ($\omega_l \tau_h < 0.01$), the spin polarization after the rapid stage is settled at some level depending on the parameters of the QD group. In this case, the Larmor precession can be neglected, and the sequence of small turnings in the Rashba fields can be considered as an effective precession around the growth direction Z. In these conditions, the S_z component is stabilized. In contrast, the transverse spin component relaxes quickly, which is why in the experiment we did not observe the rest transverse spin polarization with a long relaxation time.

The orientation dependence of the g factor allows us to add some details to the considered model. The value $g = 1.9994$ coincides, within the experimental error, with the typical g-factor value for electron states near the conduction band edge in Si [24]. The fact that the g factor stays close to this value up to $\theta \approx 30°$ confirms that the electron is located in silicon until this orientation of the magnetic field. In other words, the electron increases its localization radius remaining in silicon. After the $\theta = 30°$ point, the electron localization radius exceeds the size of the QD group, and the g factor drastically changes to the value $g = 1.9992$. Such a behavior can be explained by the change of the electron wave function penetration into the SiGe barriers surrounding the QD groups (see Fig. 10). The penetration depends on the magnetic field orientation due to the wave function shrinking effect that is more pronounced at small θ (dashed line in Fig. 10) than at large θ values (solid line in Fig. 10). The presence of Ge atoms can provide a decrease of the g factor [21].

Let us verify this assumption and estimate the value of the Ge content in the localization area of the electron providing the g-factor value $g = 1.9992$. One can write the following expression for the electron g factor:

$$g_{el} = g(\mathrm{Si})(1 - \alpha) + g(\mathrm{Ge})\alpha,$$

where α is the Ge content.

The conduction band minimum in silicon is located in the Δ point. Since the Ge content is small, we assume that in the SiGe regions the conduction band minimum is also located in the Δ point. In our previous work [21] following the approach of Liu [25] we have found the principal g-factor values for

the Δ point in germanium, $g_{\parallel}^{\mathrm{Ge}_{\Delta}} = 2.0412$, $g_{\perp}^{\mathrm{Ge}_{\Delta}} = 1.8873$. As the strain is small, for simplicity we use the value of the g factor averaged over all Δ valleys, $g(\mathrm{Ge}) = 1/3g_{\parallel} + 2/3g_{\perp} = 1.9386$. For $g(\mathrm{Si})$ we take the value of the g factor of the electron states at the conduction band edge, $g = 1.9995$. Then the resulting g factor is given by

$$g_{el} = 1.9995(1 - \alpha) + 1.9386\alpha.$$

Substituting $g_{el} = 1.9992$ we find $\alpha \approx 0.5\%$, which is a reasonable value for our experimental structures. So, at $\theta < 30^{\circ}$ the g factor of electrons localized in the structure under study is $g \approx 1.9994(5)$ which corresponds to the Ge content in the electron localization area $\alpha \approx 0$. At $\theta > 30^{\circ}$ the g factor of electrons is $g \approx 1.9992$ which is provided by $\alpha \approx 0.5\%$.

It should be noted that the same value of electron g factor was obtained by us in another ESR experiment for a structure with large SiGe nanodisks having a diameter of 100–150 nm. For this structure we used a substrate with specially created nucleation sites to obtain a more ordered array of quantum dots. These nucleation sites originated due to strain modulation in the surface layer induced by previously buried QDs. Large dome-shaped clusters grown at a previous stage at a temperature of 650° have a good spatial ordering due to a long-range elastic interaction between the QDs [15]. On this strain-modulated surface we have grown 10 layers of QDs using the same temperature regime as in the structure under study ($T = 550\,^{\circ}$C for the QD growth and $T = 500\,^{\circ}$C for the overgrowth by Si). However, we reduce the amount of deposited Ge down to 4 ML in each QD layer, and, as a result, we obtain a well ordered array of nanodisks after the overgrowth with Si. Thus, we can compare two structures: (1) a nonordered array with groups of closely spaced QDs, and (2) a well ordered array of nanodisks, one nanodisk instead of one QD group. The average size of QD groups coincides with the characteristic size of nanodisks.

The ESR data obtained on the test structure with nanodisks confirm the model proposed in this work. The ESR signal has an isotropic g factor $g = 1.9992 \pm 0.0001$ and an isotropic ESR line width $\Delta H_{pp} \approx 0.4$ Oe. The absolute value of the g factor is the same as in the structure with QD groups at $\theta > 30^{\circ}$. This can be explained by the identical electron localization radius and identical temperature regime of the QD creation. The last factor determines the GeSi intermixing and strain in the QD system, which have a high influence on the g-factor value. The isotropy of the ESR line is explained by the absence of tunneling transitions between nanodisks which are well ordered in the plane of QD array and positioned at equal distances (~100 nm) from each other. The narrowness of the ESR line indicates a high averaging efficiency of nuclear magnetic fields by the electron state with a large localization radius and the high uniformity of the array of nanodisks (negligible inhomogeneous broadening). In the structure with QD groups the averaging by means of tunneling between the dots is not so efficient, so that we observe a few times larger ESR line width.

V. CONCLUSION

In summary, we demonstrate that the existence of closely spaced QD groups provides an increase of the spin relaxation time in the QD system. Changing the electron localization radius by an external magnetic field allows us to catch the effect of the ESR line narrowing and to obtain, at a special orientation of the magnetic field, a fourfold increased relaxation time T_1 as compared to the case of the recently studied homogeneous QD arrays.

ACKNOWLEDGMENTS

This work was supported by RFBR (Grants No. 11-02-00629-a and No. 13-02-12105), SB RAS integration project No. 83 and DITCS RAS project No. 2.5, as well as by the FCT of Portugal through the projects PEst-C/CTM/LA0025/2011, RECI/FIS-NAN/0183/2012, and the European FP7 project Mold-Nanonet.

[1] I. Žutić, J. Fabian and S. Das Sarma, Rev. Mod. Phys. **76**, 323 (2004).
[2] D. Loss and D. P. DiVincenzo, Phys. Rev. A **57**, 120 (1998); B. E. Kane, Nature (London) **393**, 133 (1998).
[3] M. Kroutvar, Y. Ducommun, D. Heiss, M. Bichler, D. Schuh, G. Abstreiter, and J. Finley, Nature (London) **432**, 81 (2004).
[4] A. F. Zinovieva, A. V. Dvurechenskii, N. P. Stepina, A. I. Nikiforov, A. S. Lyubin, and L. V. Kulik, Phys. Rev. B. **81**, 113303 (2010).
[5] Y. A. Bychkov and E. I. Rashba, J. Phys. C **17**, 6039 (1984).
[6] M. I. Dyakonov and V. I. Perel', Sov. Phys. Solid State **13**, 3023 (1972).
[7] A. F. Zinovieva, A. V. Nenashev, and A. V. Dvurechenskii, *Nanostructures: Physics and Technology*, Proceedings of 18th International Symposium (Ioffe Physical-Technical Institute, St. Petersburg, 2010), p. 191.
[8] B. I. Shklovskii, Phys. Rev. B **73**, 193201 (2006).
[9] R. I. Dzhioev, K. V. Kavokin, V. L. Korenev, M. V. Lazarev, B. Ya. Meltser, M. N. Stepanova, B. P. Zakharchenya, D. Gammon, and D. S. Katzer, Phys. Rev. B **66**, 245204 (2002).
[10] I. N. Stranski and L. Krastanow, Sitzungsber. Akad. Wiss. Wien, Math.-Naturwiss. Kl., Abt. 2B **146**, 797 (1938).
[11] A. I. Yakimov, A. V. Dvurechenskii, N. P. Stepina, A. V. Nenashev, and A. I. Nikiforov, Nanotechnology **12**, 441 (2001).
[12] A. I. Yakimov, A. V. Dvurechenskii, A. I. Nikiforov, A. A. Bloshkin, A. V. Nenashev, and V. A. Volodin, Phys. Rev. B **73**, 115333 (2006).
[13] A. Schweiger and G. Jeschke, *Principles of Pulse Electron Paramagnetic Resonance* (Oxford University Press, Oxford, 2001).
[14] C.-H. Lee, Y.-Y. Shen, C. W. Liu, S. W. Lee, B.-H. Lin, and C.-H. Hsu, Appl. Phys. Lett. **94**, 141909 (2009).
[15] G. Capellini, M. De Seta, F. Evangelisti, V. A. Zinovyev, G. Vastola, F. Montalenti, and Leo Miglio, Phys. Rev. Lett. **96**, 106102 (2006).

[16] B. I. Shklovskii and A. L. Efros, *Electronic Properties of Doped Semiconductors* (Springer, Berlin, 1984).
[17] F. J. Dyson, Phys. Rev. **98**, 349 (1955).
[18] Z. Wilamowski and W. Jantsch, Phys. Rev. B **69**, 035328 (2004).
[19] A. F. Zinov'eva, A. V. Nenashev, and A. V. Dvurechenskii, JETP Lett. **82**, 302 (2005).
[20] C. P. Slichter, *Principles of Magnetic Resonance* (Springer-Verlag, Berlin, 1978).
[21] A. F. Zinovieva, A. V. Dvurechenskii, N. P. Stepina, A. S. Deryabin, A. I. Nikiforov, R. M. Rubinger, N. A. Sobolev, J. P. Leitao, and M. C. Carmo, Phys. Rev. B **77**, 115319 (2008).
[22] A. F. Zinovieva, A. V. Nenashev, and A. V. Dvurechenskii, Phys. Rev. B **71**, 033310 (2005).
[23] A. M. Tyryshkin, S. A. Lyon, W. Jantsch, and F. Schäffler, Phys. Rev. Lett. **94**, 126802 (2005).
[24] C. F. Young, E. H. Poindexter, G. J. Gerardi, W. L. Warren, and D. J. Keeble, Phys. Rev. B **55**, 16245 (1997).
[25] L. Liu, Phys. Rev. **126**, 1317 (1962).